Journal of Sound and Vibration 326 (2009) 540–556

Contents lists available at ScienceDirect

Journal of Sound and Vibration

journal homepage: www.elsevier.com/locate/jsvi

Identification of vibration excitations from acoustic measurements using near field acoustic holography and the force analysis technique

C. Pézerat [a,*], Q. Leclère [a], N. Totaro [a], M. Pachebat [b]

[a] LVA, INSA-Lyon, 25 bis avenue Jean Capelle, F-69621 Villeurbanne Cedex, France
[b] R&D Acoustics and Vibration, PSA Peugeot Citroën, Vélizy-Villacoublay F-78943, France

ARTICLE INFO

Article history:
Received 19 November 2008
Received in revised form
29 April 2009
Accepted 5 May 2009
Handling Editor: C.L. Morfey
Available online 31 May 2009

ABSTRACT

This study presents a method of using acoustic holography and the force analysis technique to identify vibration sources from radiated noise measurements. The structure studied is a plate excited by a shaker on which three measurements were performed: the first is a reference measurement of plate velocity obtained by scanning laser vibrometry, the second is based on sound pressure measurements in the near field of the structure, and the third is the measurement of normal acoustic velocities by using a p-U probe recently developed by Microflown Technologies. This was followed by the application of classical NAH, known as pressure-to-velocity holography and velocity-to-velocity holography to predict the plate velocity field from acoustic measurements at distances of 1 and 5 cm. Afterwards, the force analysis technique, also known as the RIFF technique, is applied with these five data sets. The principle is to inject the displacement field of the structure into its equation of motion and extract the resulting force distribution. This technique requires regularization done by a low-pass filter in the wavenumber domain. Apart from pressure-to-velocity holography at 5 cm, the reconstructed force distribution allows localizing the excitation point in the measurement area. FAT regularization is also shown to improve results as its cutoff wavenumber is optimized with the natural wavenumber of the plate. Lastly, quantitative force values are extracted from force distributions at all frequencies of the band 0–4 kHz studied and compared with the force spectrum measured directly by a piezoelectric sensor.

© 2009 Elsevier Ltd. All rights reserved.

1. Introduction

The general aim of the study described in this paper is to identify the excitations generating the vibration and the acoustic radiation of a structure by contactless measurements. The approach followed is particularly interesting because it allows detecting the mechanical cause of the radiated noise. The objective is to go further than simple airborne source characterization, as structure-borne noise source characterization is also concerned. Consequently, the quantities sought are mechanical forces or moments, force distribution and/or the mechanical power applied to the structure. To achieve this, two well known methods are coupled: near field acoustic holography (NAH) and the force analysis technique (FAT).

For several years, NAH has proved a useful technique for the acoustic source identification in terms of pressure and/or velocity field prediction [1–3]. In its usual form, the principle consists in measuring sound pressure on a microphone grid on a given plane, calculating the pressure field in the *k*-space by a 2D Fourier transform and computing "acoustic back-propagation" by using the inverse solution of the wave equation in the normal direction of the plane. As in several inverse

* Corresponding author. Fax: +33 4 72 43 87 12.
E-mail address: charles.pezerat@insa-lyon.fr (C. Pézerat).

0022-460X/$ - see front matter © 2009 Elsevier Ltd. All rights reserved.
doi:10.1016/j.jsv.2009.05.010

problems, the NAH is particularly sensitive to measurement uncertainties. This ill-posed problem characteristic is due to the fact that small data errors are essentially located in the high wavenumber domain, amplified by the back-propagation process. That is the reason why wavenumber low-pass filtering is essential in NAH.

The force analysis technique is a method first developed 10 years ago by Pezerat [4,5]. It is also known as the RIFF technique, the acronym stemming from the French Résolution Inverse Filtrée Fenêtrée (filtered windowed inverse resolution). It is intended to compute the force distribution acting on a structure by using the measurement of its displacement field. Here, computation of force distribution is based on the use of the vibration equation of motion where the spatial derivatives of the displacement field are deduced by finite difference schemes. As with NAH, this approach is highly sensitive, so wavenumber low-pass filtering is also required. This filtering is done by using a convolution product of the reconstructed force distribution and a finite spatial response of a low-pass wavenumber filter. It should be noted that this approach is relatively local and that knowledge of the equation of motion is sufficient. Measurements of the entire structure are not needed and the boundary conditions can be unknown. Also, it is possible to identify every type of excitation, since they can be extracted if the force distribution is known. For example, it is possible to identify point forces [6], moments [7], injected power [8], etc. Until now, FAT has been developed for simple structures such as beams [6], plates [5] and shells [9,10] where the equation of motion is known analytically.

In this work, the example chosen is a plate excited by a shaker and the goals are to localize and identify the applied force. Different kinds of data were measured in order to compare the accuracies of several approaches. First, the displacement field of the plate was measured directly by a scanning laser vibrometer. This provides a reference measurement through the use of the classical RIFF method. Several distances are proposed for the acoustic measurements. Traditionally, sound pressure is used in NAH because it is easier to measure sound pressure than particle velocity. A Microflown p-U transducer is now available [11–13] that gives sound pressure and acoustic particle velocity in the direction normal to the plate. The velocity component in this direction is most important [14]; the velocity components in the plane parallel to the plate are already fairly well represented in the pressure measurements, while the velocity component in the normal direction must be deduced from theory if it is not measured experimentally. The use of this p-U transducer in the NAH gives better results as predicted quantity (velocity) is the same as that measured [14,15].

Excluding the conclusion, the rest of this paper is divided into three parts. The first part contains the description of the experiments where data samples are shown. The second part presents the method of performing the back-propagations and gives the identified velocity fields of the plate. The last part concerns force identification by using FAT, where data from the laser vibrometer, pressure-to-velocity NAH predictions and velocity-to-velocity NAH predictions are used. Finally, force spectra are compared with the force spectrum measured by a piezoelectric sensor.

2. Experimental procedures

2.1. Experimental setup

These measurements are intended to provide satisfying results, thereby demonstrating the ability of the NAH and FAT methods to localize and quantify the excitation acting on a structure. Because the structure must be capable of radiation (acoustic measurement) and because its analytic equation of motion must also be known (in order to use FAT), it appeared that a plate was the simplest structure that could be used. More specifically, it was a 5 mm thick aluminium plate clamped by three screws fixed at the top of the setup (see Fig. 1).

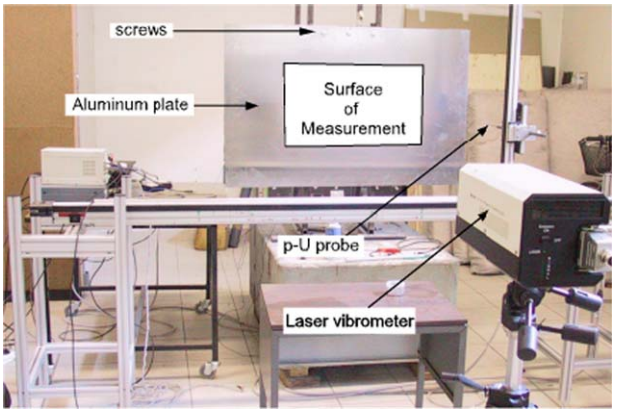

Fig. 1. Experimental setup.

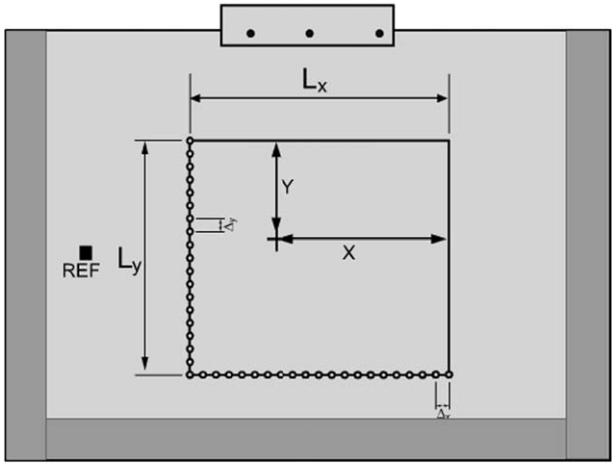

Fig. 2. Grid of measurements (399 points): 21 points separated by Δ_x located on length L_x; 19 points separated by Δ_y located on length L_y. The position of the point force is $(X, Y) = (-275\,\text{mm}, -214\,\text{mm})$. REF represents the position of the reference accelerometer. Dark gray surfaces illustrate the positions of absorbing bands.

The same 2D grid was used for all the measurements (structural and acoustic measurements). This grid is represented in Fig. 2. It is composed of:

- 21 points in the x direction (length $L_x = 430\,\text{mm}$) separated by $\Delta_x = 21.5\,\text{mm}$.
- 19 points in the y direction (length $L_y = 387\,\text{mm}$) separated by $\Delta_y = 21.5\,\text{mm}$.

For the phase reference of all measurements, an accelerometer was fixed to the plate outside the grid of measurement points.

Moreover, the plate was excited by an electrodynamic shaker driven by white noise and located in the grid at position $(X, Y) = (-275\,\text{mm}, -214\,\text{mm})$ (see Fig. 2). The force applied by the shaker was measured directly by a piezoelectric sensor. This allows providing a reference for the final FAT predictions.

Finally, to avoid high resonances at which FAT can give poor results for the corresponding eigenfrequencies (see [5]), the modal overlap of the plate was increased by absorbing bands fixed near its boundaries.

2.2. Plate velocity field measurement

The aim of the plate velocity field measurement is to give a reference for force identification by using back-propagation techniques. The plate velocity field was measured with a scanning Polytec laser vibrometer at each point of the grid presented in Fig. 2. For each point, auto spectra, transfer functions and coherences between each sensor (laser, accelerometer, force sensor) were recorded in the frequency range (5–4000 Hz) with a step Δf equal to 5 Hz. The averaged coherence (defined as the ratio between averaged coherent power output spectrum and averaged output power spectrum [16]) between plate velocity (laser vibrometer) and force (force sensor) is presented in Fig. 3. As can be seen, coherence decreases above 2500 Hz due to the low velocity level at high frequency.

2.3. Pressure and acoustic velocity field measurement

The sound pressure and the acoustic velocity fields are the input data for the back-propagation techniques used to estimate plate velocity. These measurements were done by a Microflown p-U probe [12,13] where the same signal processing parameters were kept (frequency range: (5–4000 Hz); step: $\Delta f = 5\,\text{Hz}$). Also, two different distances from the plate were chosen: 1 and 5 cm.

Fig. 4 compares pressure and acoustic velocity to background noise. Pressure and velocity levels appear very high (more than 10 dB higher) compared to background noise on the frequency band 500–4000 Hz. In addition, averaged coherence between signals given by the p-U sensor and the force sensor presented in Fig. 5 demonstrates that the acoustic quantities are well correlated to the point force for both distances.

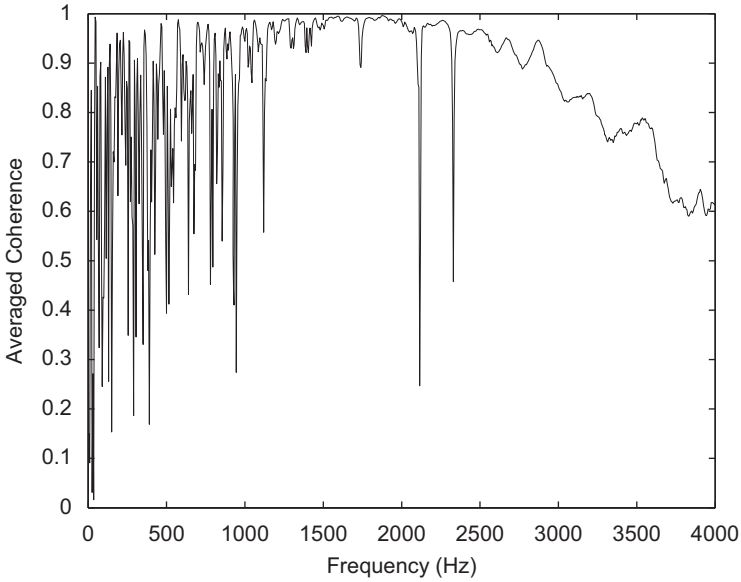

Fig. 3. Averaged coherence between the laser vibrometer and the force sensor defined as the ratio between coherent output power spectrum and output power spectrum.

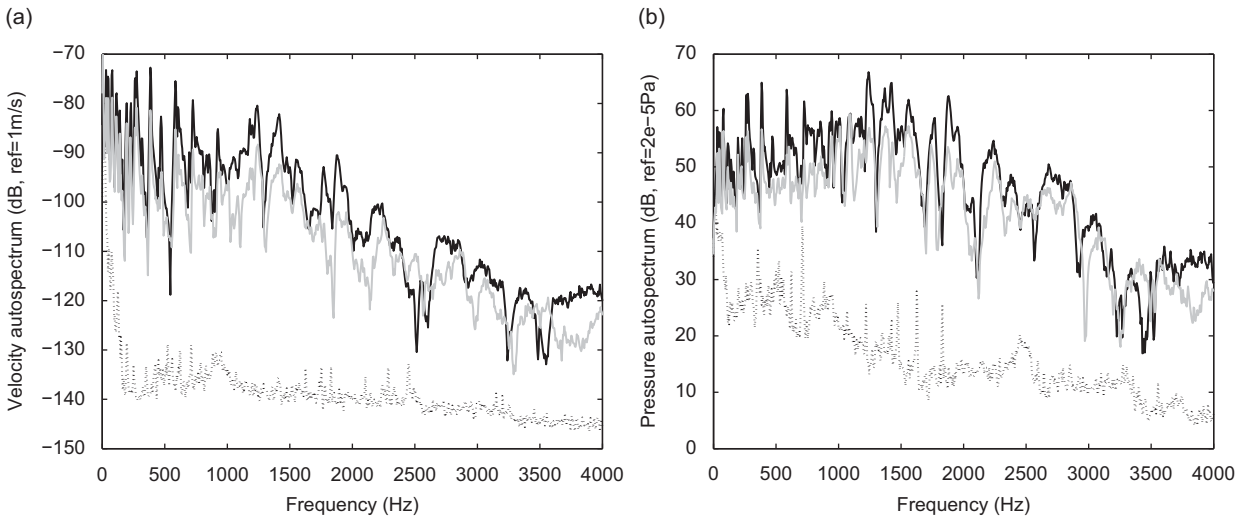

Fig. 4. Influence of background noise on pressure and acoustic velocity measurements: (a) acoustic velocity autospectrum and (b) pressure autospectrum. Dot line: background noise; solid black line: 1 cm measurement; solid gray line: 5 cm measurement.

2.4. Comparison of velocity fields

In this section, averaged velocity and velocity maps measured by the scanning laser vibrometer, by the p-U probe at 1 cm and by the p-U probe at 5 cm are compared.

Figs. 6 and 7 show the quality of acoustic measurements. In Fig. 6, curves corresponding to the plate velocity and the acoustic velocity at 1 cm seems to be very close. Indeed, the difference does not exceed 2 dB. For applications that focus only on analyzing the velocity field of the plate, this small difference could be considered as a continuity relationship.

However, at 5 cm the difference between both curves reaches more than 8 dB in the 500–2000 Hz frequency range. In this case, the level of averaged acoustic velocity is lower, because the influence of evanescent waves is less.

Fig. 7 compares velocity maps (each map has its own scale) measured with the laser vibrometer and the p-U probe at 1500 Hz. The p-U probe at 1 cm gives velocity maps very close to those measured by the laser vibrometer. At 5 cm, the acoustic velocity map is smoothed, although the correlation with the plate velocity is obvious.

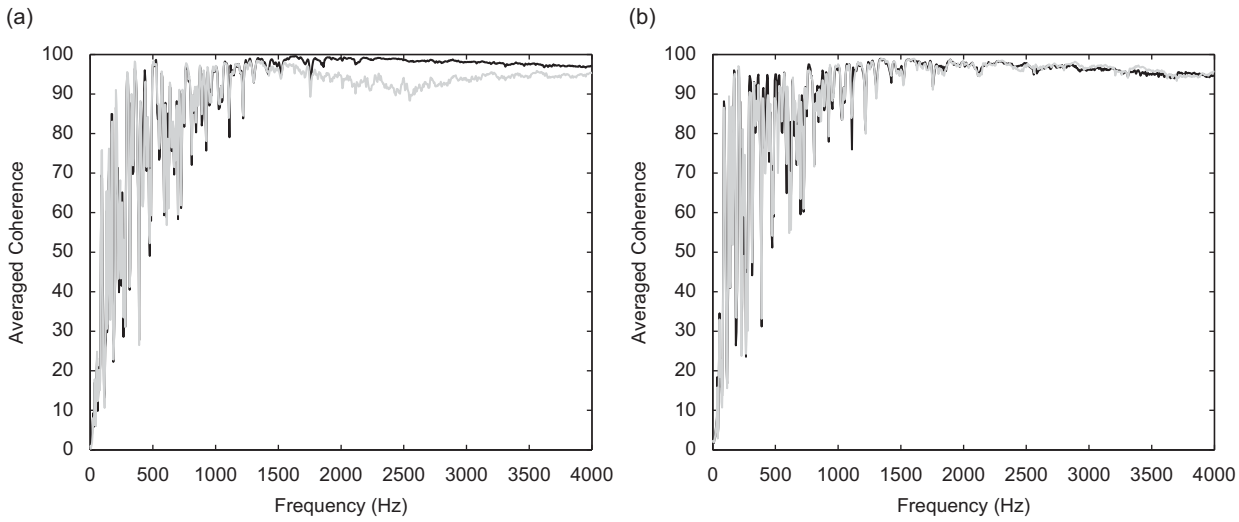

Fig. 5. Averaged coherence defined as the ratio between coherent output power spectrum and output power spectrum: (a) between acoustic velocity sensor and force sensor and (b) between pressure sensor and force sensor. Solid black line: 1 cm measurement; solid gray line: 5 cm measurement.

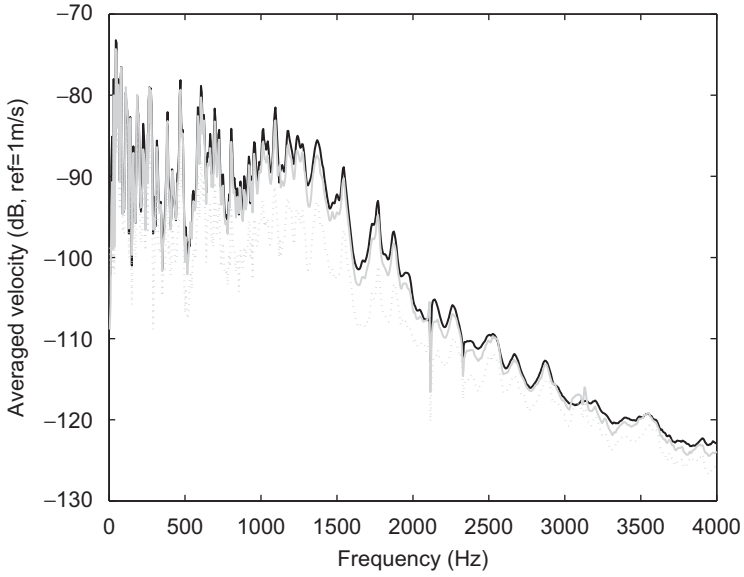

Fig. 6. Space averaged velocity. Solid black line: laser vibrometer; solid gray line: p-U probe at 1 cm; dot gray line: p-U probe at 5 cm.

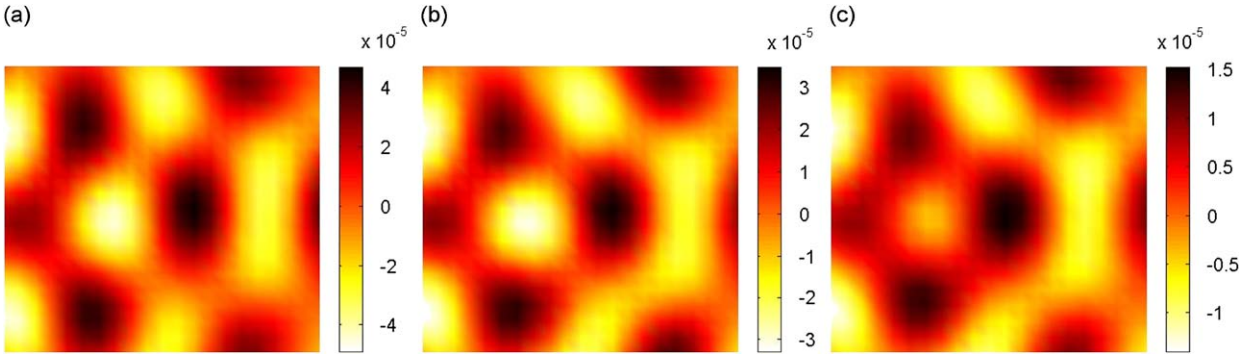

Fig. 7. Velocity maps at 1500 Hz: (a) laser vibrometer; (b) p-U probe at 1 cm from the plate and (c) p-U probe at 5 cm from the plate. Each map has its own scale.

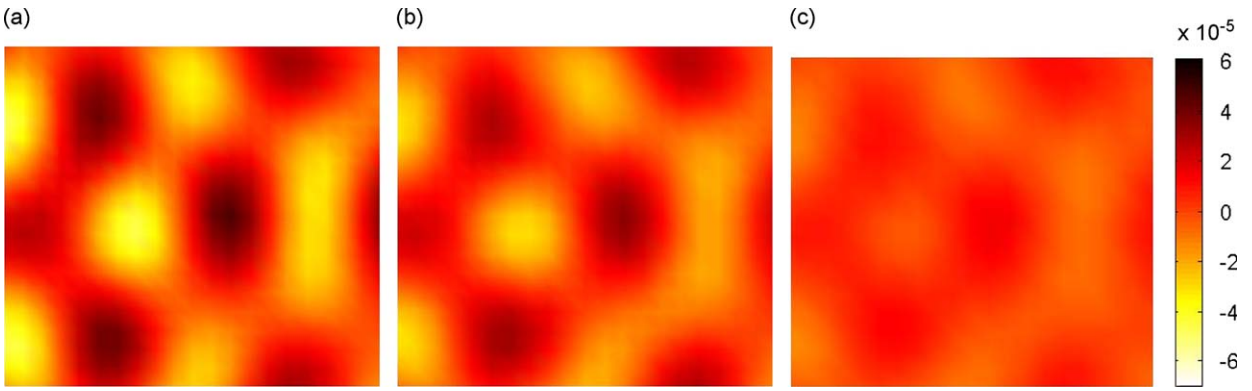

Fig. 8. Velocity maps at 1500 Hz: (a) laser vibrometer; (b) p-U probe at 1 cm from the plate and (c) p-U probe at 5 cm from the plate. Maps have the same scale.

Fig. 8 shows these maps in the same scale. In this case, the influence of distance is clearly shown. This figure demonstrates that velocity back-propagation is needed.

3. Acoustic pressure and velocity back-propagations

3.1. Basics

In this section a back-propagation correction is proposed to assess the velocity of the plate from acoustic quantities. Acoustical holography [1] is based on a 2D discrete Fourier transform (DFT) of acoustical information measured on a plane in the near field of an acoustic source. The data measured are usually sound pressures, but holography can easily be formulated with acoustic velocities measured in the normal direction of the measurement plane [14]. Assuming the periodicity of the acoustic fields in the measurement plane and a harmonic time dependence $e^{-j\omega t}$, the acoustic pressure is expressed in Fourier series:

$$p(x,y,z) = \sum_n \sum_m P_{nm}(z)\, e^{jk_{nx}x}\, e^{jk_{my}y} \tag{1}$$

where $k_{nx} = 2\pi n/L_x$, $k_{my} = 2\pi m/L_y$, L_x and L_y stand for x and y dimensions of the measurement grid and n, m are orders of the Fourier components varying between the limits fixed by the spatial resolution.

Taking only waves travelling towards positive values of z, the use of (1) in the Helmholtz equation $\Delta p + (\omega/c)^2 p = 0$ allows identifying the form of $P_{nm}(z)$:

$$\begin{aligned} &P_{nm}(z) = P_{nm}(0)\, e^{jk_{nm}z} \\ &\quad \text{with } k_{nm} = \sqrt{(\omega/c)^2 - k_{nx}^2 - k_{my}^2} \quad \text{for } (\omega/c)^2 \geq k_{nx}^2 + k_{my}^2 \\ &\quad k_{nm} = j\sqrt{k_{nx}^2 + k_{my}^2 - (\omega/c)^2} \quad \text{for } (\omega/c)^2 \leq k_{nx}^2 + k_{my}^2 \end{aligned} \tag{2}$$

where ω is the pulsation (rad/s) and c the speed of sound (m/s).

Thus, each Fourier component in any plane z can be easily predicted from the values in the measurement plane at $z = 0$. Now, by considering the Euler equation giving the relationship between the acoustic velocity and the acoustic pressure gradient, Eq. (2) can be written in terms of normal acoustic velocity:

$$V_{nm}^z(z) = \frac{j}{\rho\omega} \nabla P_{nm}(z) = \frac{k_{nm}}{\rho\omega} P_{nm}(0)\, e^{jk_{nm}z} = V_{nm}^z(0)\, e^{jk_{nm}z} \tag{3}$$

This equation allows assessing the normal acoustic velocity in the plate plane from either the normal acoustic velocity or the pressure in the measurement plane at $z = 0$.

3.2. Regularization filters and extra-padding solutions

3.2.1. Back-propagation filter

For back-propagation applications, z is negative in Eq. (3). Thus, the exponential operator in Eq. (3) is either harmonic if k_{nm} is real, or increasing exponentially if k_{nm} is imaginary, corresponding to the back-propagation of evanescent waves. This latter operation is particularly sensitive to measurement errors and a filtering operation is necessary to minimize them. High wavenumbers of the hologram that would be amplified by more than the gain G_R are attenuated, since the

wavenumbers of the 2D DFT components are given by $\sqrt{k_{nx}^2+k_{my}^2}$. This is a low-pass filter adapted to the back-propagation distance and to the frequency. The corresponding cutoff wavenumber k_c^R can be written as follows:

$$k_c^R=\sqrt{\left(\frac{\log(10)G_R}{z.20}\right)^2+(\omega/c)^2} \tag{4}$$

where G_R is the maximum gain in dB of the retro-propagation operator.

The shape of the k-space filter is similar to the filter described in [17].

3.2.2. Pressure-to-velocity filter

The computation of the normal acoustic velocity in the measurement plane from acoustic pressures can also amplify measurement noise. The pressure-to-velocity operation described in Eq. (3) is performed by multiplying the pressure components P_{nm} by the ratio $k_{nm}/\rho\omega$, leading to a considerable gain for high spatial frequencies. A maximum gain G_{PV} is fixed for the pressure-to-velocity operation. This gain is given relatively to the pressure-to-velocity correction of the plane wave, i.e. ρc. The cutoff wavenumber k_c^{PV} for the corresponding low-pass filter is given by

$$k_c^{PV}=\frac{\omega}{c}\sqrt{1+10^{G_{PV}/10}} \tag{5}$$

where G_{PV} is the maximum gain in dB of the pressure-to-velocity operator.

The pressure-to-velocity filter is combined in this work with the back-propagation filter when acoustic pressures are used as the input data.

3.2.3. Extrapolation of the acoustic fields

There is a very strong assumption of the periodicity of the acoustic field when using DFT. Artificial discontinuities produced at the edges of the measurement domain induce artifacts affecting the entire wavenumber domain. The use of low-pass filters is insufficient, as they lead to "wraparound" errors (see [2]). The usual approach for solving this problem is to weight the domain by Hanning or Tukey windows to constrain values at boundaries to zero. This windowing is appreciable when the measurement domain is significantly larger than the source, but windowing can have a very penalizing effect when the measurement domain has the same size as the source, as it is in this study. To limit the bias error caused by windowing, the domain is extended by extrapolation carried out on the acoustic fields. This spatial extension is not a new idea, but usually zero-padding is used (see [2]). Some iterative extrapolation approaches are proposed in the literature [18]. The idea is to apply a low-pass filter in the wavenumber domain to the zero-padded hologram. This operation not only attenuates the discontinuities at the boundaries of the hologram, it also corrupts measured data. The measurements are then re-injected into the filtered hologram, keeping only changes outside the measurement surface, and the low-pass filter is applied repeatedly to finally obtain the extrapolation. In this work, the

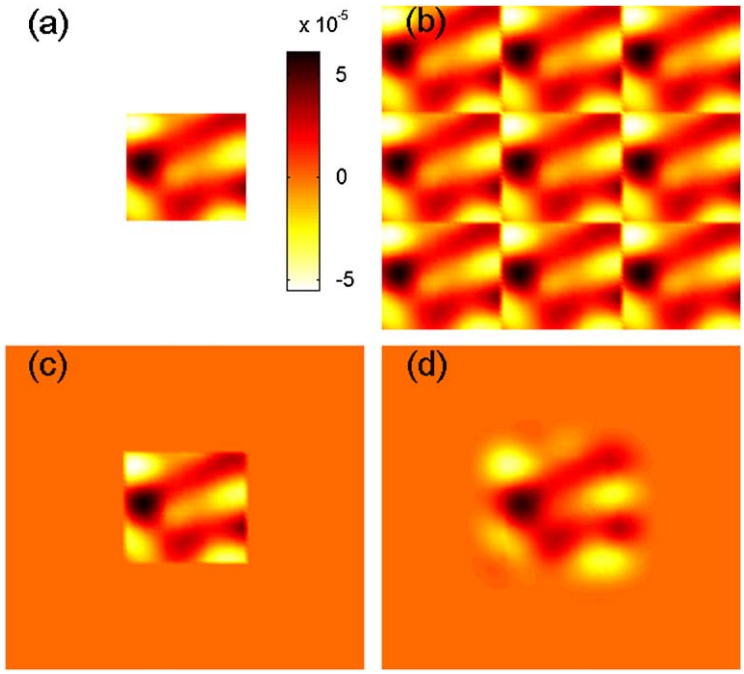

Fig. 9. (a) Measured acoustic velocity at 890 Hz. (b) Periodized field using the DFT. (c) Classic 100 percent zero-padding. (d) Used extrapolation.

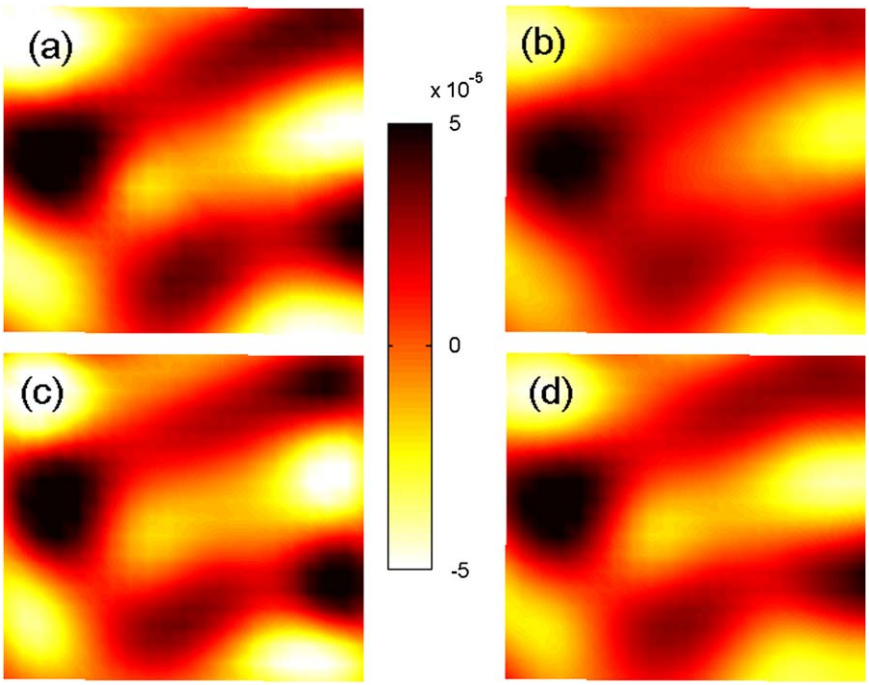

Fig. 10. (a) Plate velocity at 890 Hz measured by the laser vibrometer. (b) Measured acoustic velocity at 5 cm (multiplied by 2 to fit the color scale of other maps). (c) Back-propagated velocity with 100 percent zero-padding. (d) Back-propagated velocity with 100 percent extra-padding.

iterative process is stopped either when the difference between the filtered and unfiltered hologram is less than a given threshold, or when the iteration has reached a given maximum value. The low-pass filter used for the extrapolation is the same as that used for the retro-propagation and pressure-to-velocity operations described in the previous section. An example of extra-padding is given in Fig. 9 for the acoustic velocity field measured at 890 Hz.

Fig. 10 shows the efficiency of the chosen extrapolation solution at 890 Hz. In this example, the number of points is trebled in all directions. Edge errors are clearly visible when using classical zero-padding. The result using extrapolation is closer to the plate velocity measured directly by the laser vibrometer.

The quality of acoustic holography results can be quantified using a quadratic error indicator. The indicator chosen was defined in frequency bands by the magnitude of the difference between laser measurements and holography results divided by the magnitude of the laser measurements:

$$\varepsilon([f_l,f_s]) = \frac{\sum_{f=f_l}^{f_s}\sum_{x=1}^{N}\sum_{y=1}^{M}|v^{\text{laser}}(x,y,f)-v^{\text{holo}}(x,y,f)|^2}{\sum_{f=f_l}^{f_s}\sum_{x=1}^{N}\sum_{y=1}^{M}|v^{\text{laser}}(x,y,f)|^2} \tag{6}$$

where $[f_l,f_s]$ represents the given frequency band, N and M are the number of points in the measurement grid along the x and y directions, v^{laser} is the plate velocity measured by the laser vibrometer and v^{holo} is the acoustic velocity measured with the Microflown p-U probe back-propagated on the plate.

It is clear that it is not possible to reach a perfect match between grids used for laser and robot measurements, resulting in a residual bias error contributing to the quadratic error indicator. Meanwhile, the holography results are all computed from data acquired on the robot grid, and are compared to a unique reference velocity map obtained on the laser grid. The bias error contribution can thus be supposed equivalent for all quadratic error curves shown in following figures.

The quadratic error is shown in Fig. 11 for the velocity back-propagated without zero-padding, with 100 percent zero-padding and with 100 percent extra-padding. The error obtained with the extrapolation is between 1.5 and 2 times lower than the error with classical zero-padding over the whole spectrum and 2–3 times lower the error without zero-padding. This result shows the pertinence of the extrapolation chosen on the whole frequency range.

3.3. Back-propagation results

Acoustic pressures and velocities measured at 1 and 5 cm were back-propagated in the plate plane with a maximum back-propagation gain adjusted to 6 and 20 dB (for, respectively, 1 and 5 cm) and a maximum pressure-to-velocity gain to 10 dB. An illustration of data processing is given in Fig. 12 for acoustical data measured at 5 cm at 890 Hz. First of all, the

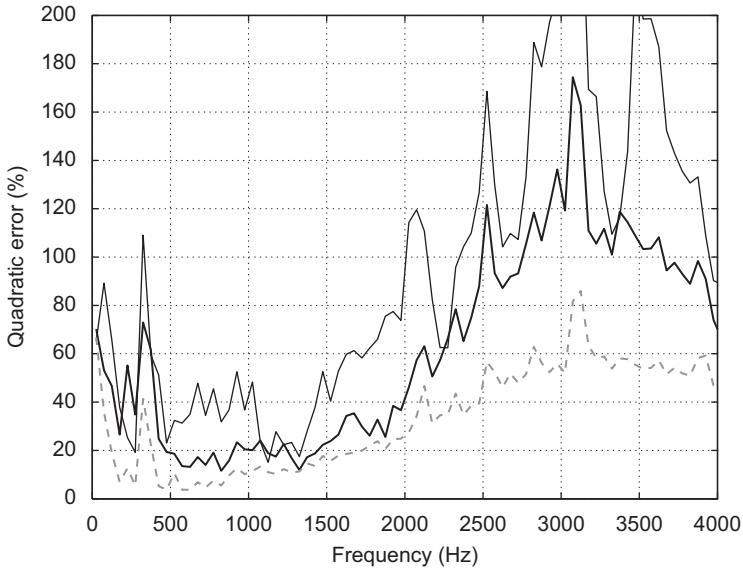

Fig. 11. Quadratic error by 50 Hz frequency bands of the holography results using acoustic velocities measured at 5 cm. Fine black: without zero-padding. Thick black: classical 100 percent zero-padding. Dotted gray: 100 percent extra-padding.

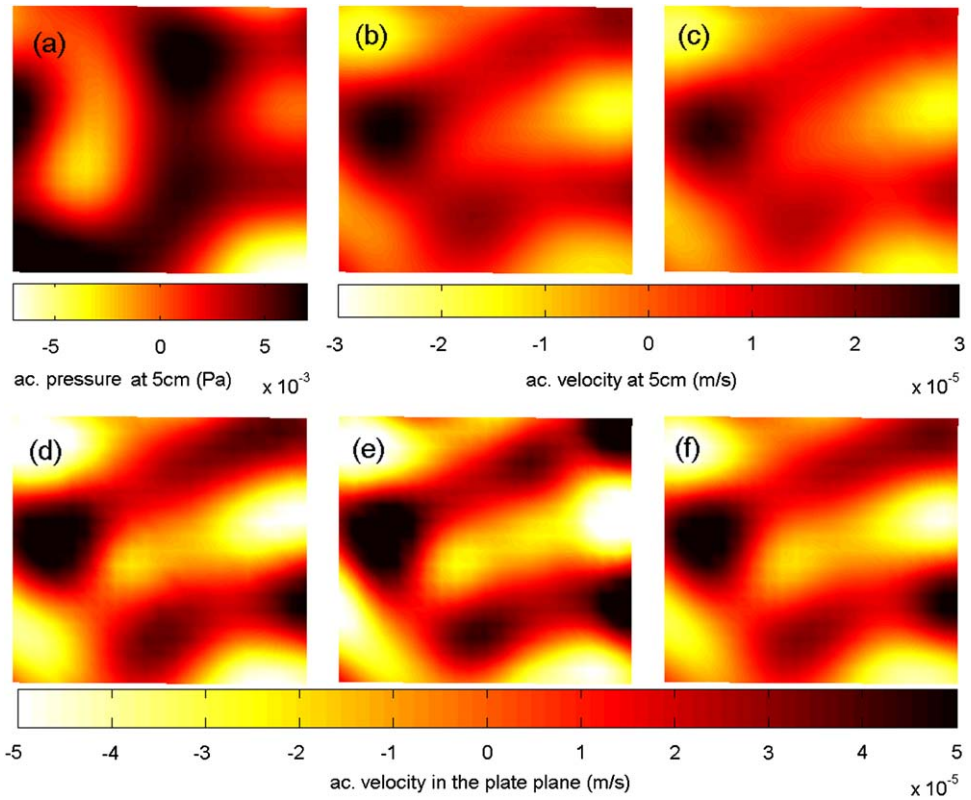

Fig. 12. (a) Acoustic pressure measured at 5 cm at 890 Hz. (b) Normal acoustic velocity at 5 cm computed using acoustic pressure measured at 5 cm. (c) Normal acoustic velocity measured at 5 cm. (d) Plate velocity measured with the laser vibrometer. (e) Computed plate velocity from measured acoustic pressure at 5 cm. (f) Computed plate velocity from measured acoustic velocity at 5 cm.

pressure map is converted into a velocity map. Then, back-propagations are applied to the resulting velocity and to the velocity measured directly by the p-U probe. Moreover, the results can be compared to the plate velocity measured directly (obtained by the laser vibrometer).

Fig. 13 shows the quadratic errors with respect to the frequency. It is clear that the results obtained at 1 cm are more reliable than those obtained at 5 cm. Also, it appears that the results obtained from the acoustic velocities are much more satisfactory than those obtained from the acoustic pressures, particularly above 1 kHz. In the extreme case, the errors computed from the pressure at 5 cm exceed 100 percent above 1500 Hz.

Regarding a hypothetical assumption of using the p-U probe as a plate velocity sensor at 1 cm without the back-propagation technique, the quadratic error associated with the velocity at 1 cm is also drawn in Fig. 13 (in gray). The comparison with the error obtained at 1 cm with acoustic holography clearly indicates that velocities are similar below 1 kHz. Otherwise, the acoustic correction should be taken into account. Indeed, with NAH, the error can be divided by 1.5 in the 1000–2500 Hz band and by more than 2 above 2500 Hz.

4. Force distribution calculation

In this section, the force distribution computation is processed by FAT [4–6]. Initially, attention is given to the spatial distribution for a given frequency in order to see if the results allow precise localization of the force applied by the shaker. Secondly, force spectra are reconstructed and compared to those measured directly by the force sensor. Finally, quantitative comparisons and frequency limits of the method are given.

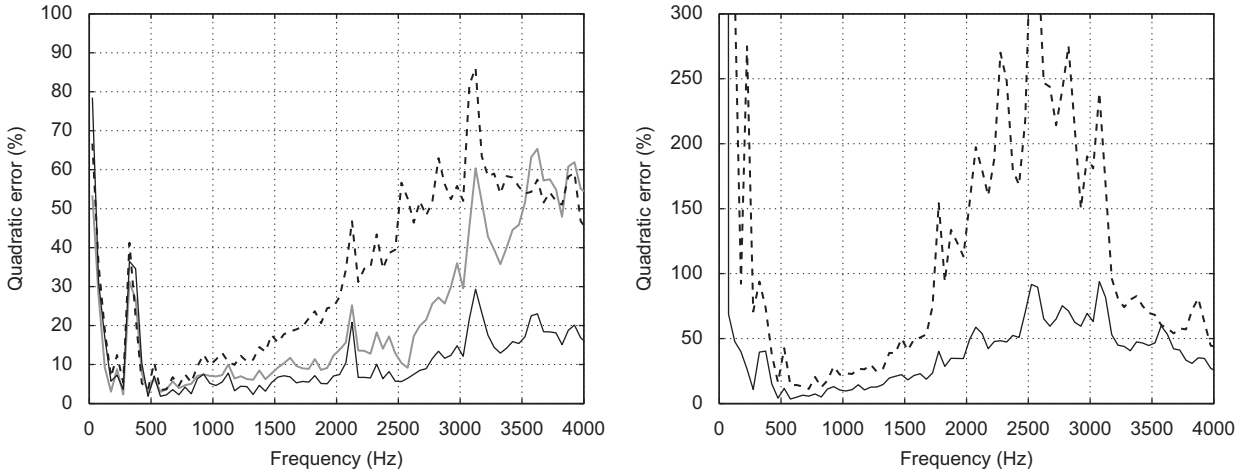

Fig. 13. Quadratic error by 50 Hz frequency bands. Solid black: back-propagated 1 cm measurement. Dotted black: back-propagated 5 cm measurements. Left: results from acoustic velocity (solid gray: measured velocity at 1 cm). Right: results from acoustic pressure.

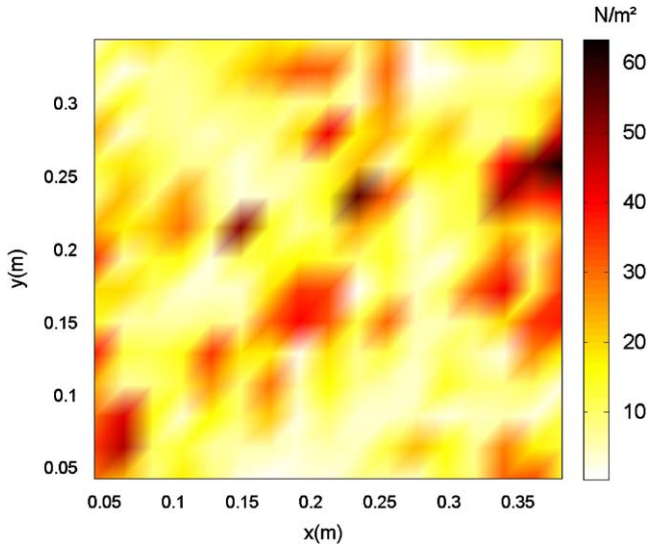

Fig. 14. Force distribution magnitude obtained from laser measurement with FAT at 890 Hz without filtering.

4.1. Using only the discretized equation of motion

The first step of the FAT method consists in injecting the displacement (measured directly or obtained from acoustic back-propagation) in the plate equation of motion discretized by a finite difference scheme. The scheme used is chosen to be an estimation of the derivatives corresponding to a truncation of a first-order Taylor series. With this approximation, the calculation of the force distribution $F_{i,j}$ at the point indices (i,j) can be computed from 13 displacements around this point:

$$F_{i,j} = \frac{Eh^3}{12(1-\nu^2)}(\delta_{i,j}^{4x} + \delta_{i,j}^{4y} + 2\delta_{i,j}^{2x2y}) - \rho h\omega^2 w_{i,j} \tag{7}$$

where E, ν, ρ, h are, respectively, the Young modulus, the Poisson ratio, the mass density and the thickness of the plate, ω is the pulsation. $w_{i,j}$ represents the displacement of the plate at point (i,j) and $\delta_{i,j}^{4x}$, $\delta_{i,j}^{4y}$ and $\delta_{i,j}^{2x2y}$ indicate the finite difference schemes approximating the spatial derivatives of the displacement. Their expressions are given in [5].

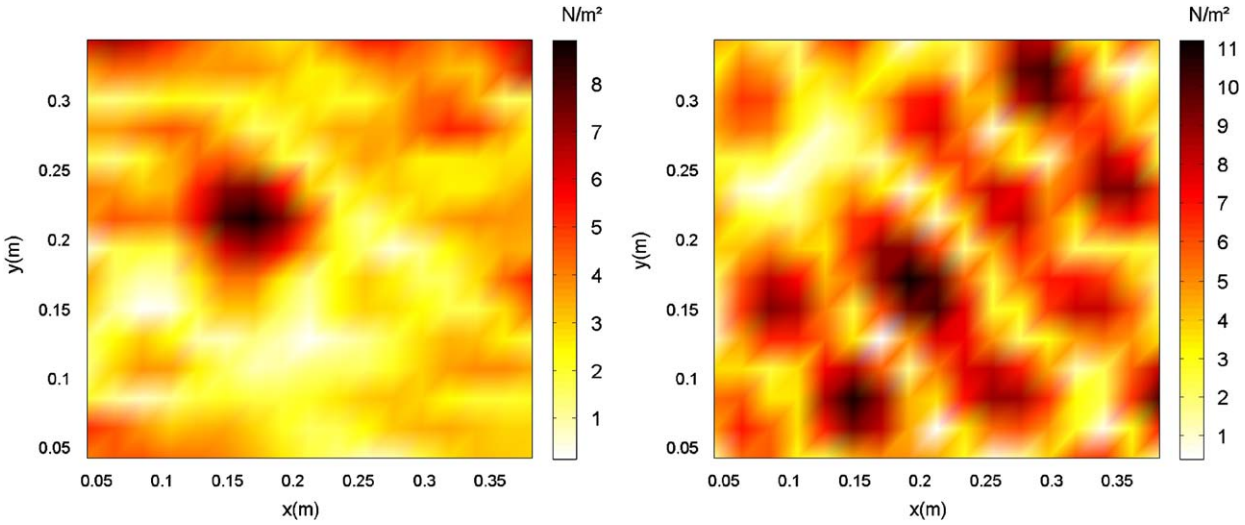

Fig. 15. Force distribution magnitude obtained with FAT at 890 Hz without filtering after pressure-to-velocity holography. Left: from pressure measurements carried out at 1 cm from the plate. Right: from pressure measurements made at 5 cm from the plate.

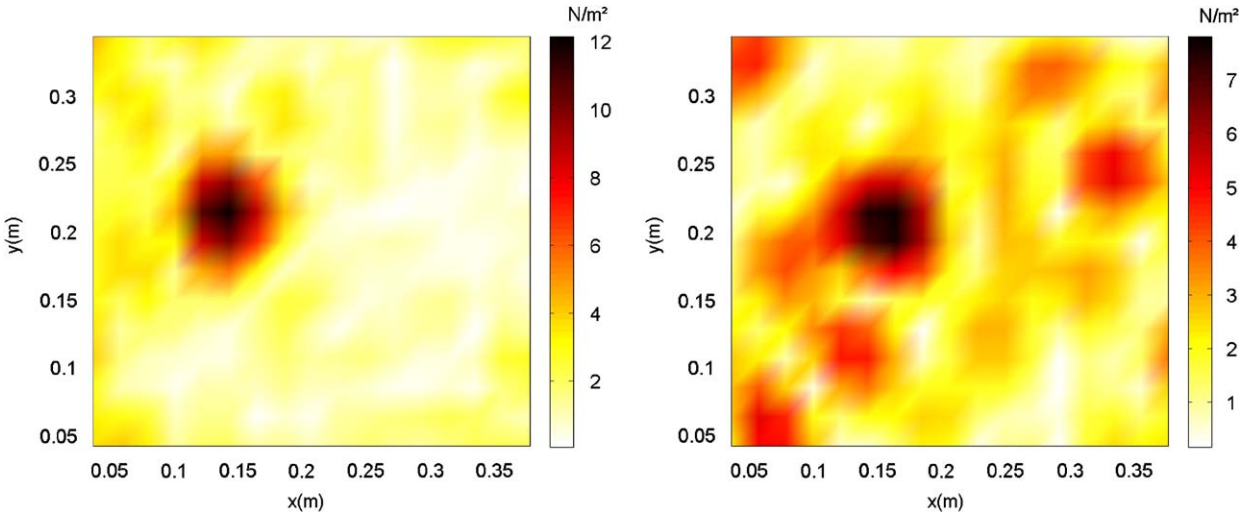

Fig. 16. Force distribution magnitude obtained with FAT at 890 Hz without filtering after velocity-to-velocity holography. Left: from velocity measurements carried out at 1 cm from the plate. Right: from velocity measurements carried out at 5 cm from the plate.

In practice, this approach cannot be used without a regularization step, because the calculation of spatial derivatives leads to a dramatic amplification of measurement errors. To illustrate this, Fig. 14 shows the force distribution obtained at 890 Hz by laser measurements. No wavenumber filtering was applied in this case, so the excitation point cannot be localized easily.

Nevertheless, the results below are proposed without filtering to see whether NAH filtering is sufficient. Fig. 15 corresponds to force distributions deduced by pressure-to-velocity holography. This result appears very interesting, because it clearly demonstrates the possibility of locating the excitation point from sound pressure measurements, although the distance between the plate and the hologram must be small. Indeed, the use of the velocity field calculated from sound pressures measured at 5 cm is not precise enough to allow good localization.

Concerning the same approach with data obtained by acoustic velocity holography, the results shown in Fig. 16 are better and the excitation is visible even at the distance of 5 cm.

4.2. Using the FAT regularization process

Even if the results locate the excitation correctly, because data have already been filtered, we propose in this section to use the usual FAT regularization to ascertain whether quality can be improved. This regularization consists in applying

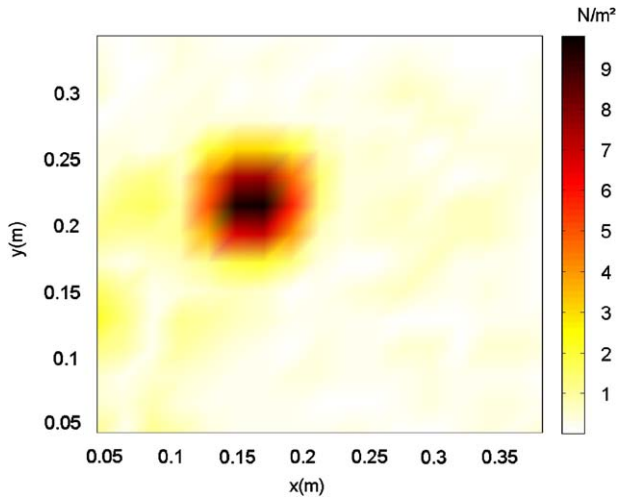

Fig. 17. Force distribution magnitude obtained with FAT at 890 Hz with $k_c^{FAT} = 2k$ from laser measurement.

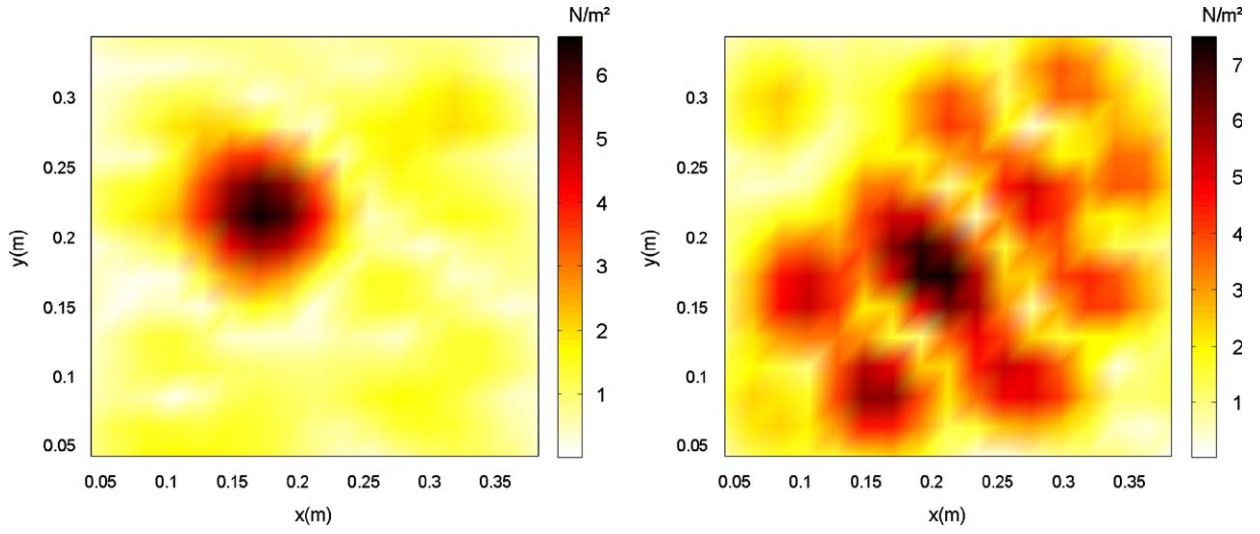

Fig. 18. Force distribution magnitude obtained with FAT at 890 Hz with $k_c^{FAT} = 2k$ after pressure-to-velocity holography. Left: from pressure measurements made at 1 cm from the plate. Right: from pressure measurements carried out at 5 cm from the plate.

windowing and low-pass wavenumber filtering [5]. In this case, the regularization parameter is the cutoff wavenumber k_c^{FAT}. Its value is chosen to follow the natural wavenumber k with a linear law $k_c^{\mathrm{FAT}} = a \cdot k$. Consequently, due to the plate dispersion equation, the cutoff wavenumber depends on the square root of the frequency:

$$k_c^{\mathrm{FAT}} = a\left(\frac{12\rho(1-\nu^2)}{E \cdot h^2}\right)^{1/4}\sqrt{\omega} \tag{8}$$

where ω is the pulsation studied and a is the FAT regularization parameter. This latter parameter depends on the noise level. Generally, it is a number between 1 and 4, but in the majority of cases $a = 2$ is a good compromise.

In this work, the window used was a Tukey window for which the force distribution was weighted at its edges over a distance equal to the cutoff wavelength $\lambda_c = 2\pi/k_c^{\mathrm{FAT}}$. The filtering was performed by a convolution product with a sinc function truncated by a Hanning window over a length of $2\lambda_c$.

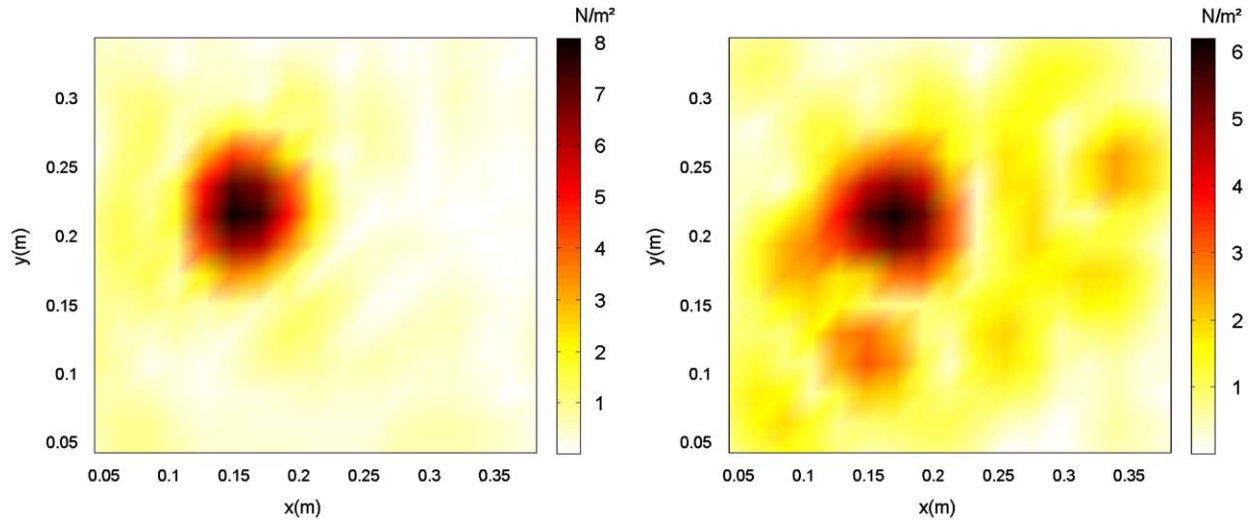

Fig. 19. Force distribution magnitude obtained with FAT at 890 Hz with $k_c^{\mathrm{FAT}} = 2k$ after velocity-to-velocity holography. Left: from velocity measurements made at 1 cm from the plate. Right: from velocity measurements carried out at 5 cm from the plate.

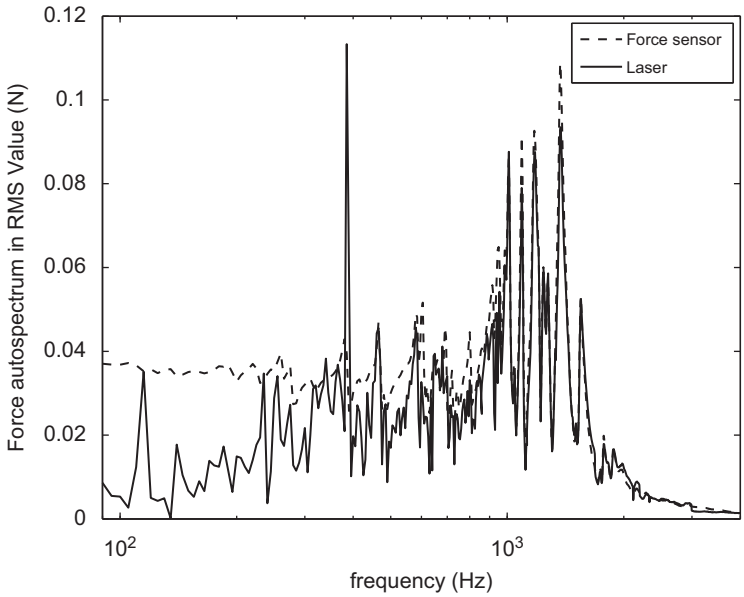

Fig. 20. Force spectra. Dotted line: measured by the piezoelectric sensor—solid line: identified by FAT from laser measurements.

Fig. 17 corresponds to the filtering of the noisy distribution illustrated in Fig. 14 with $k_c^{FAT} = 2k$ using the Tukey window and the filtering described. The good localization of the excitation point proves that the regularization parameters were well optimized.

Also, as seen in Figs. 18 and 19, the use of a cutoff wavenumber matching the FAT criteria gives results with better qualities than above, but the regularization is not sufficient for long distance pressure-to-velocity holography, because the velocity prediction is too distant from the plate velocity.

4.3. Force spectra

In this last section, the identified force spectra are described and compared to those measured directly by a piezoelectric force sensor. All the regularization parameters (maximum back-propagation gain G_R, G_{PV}, FAT regularization parameter a)

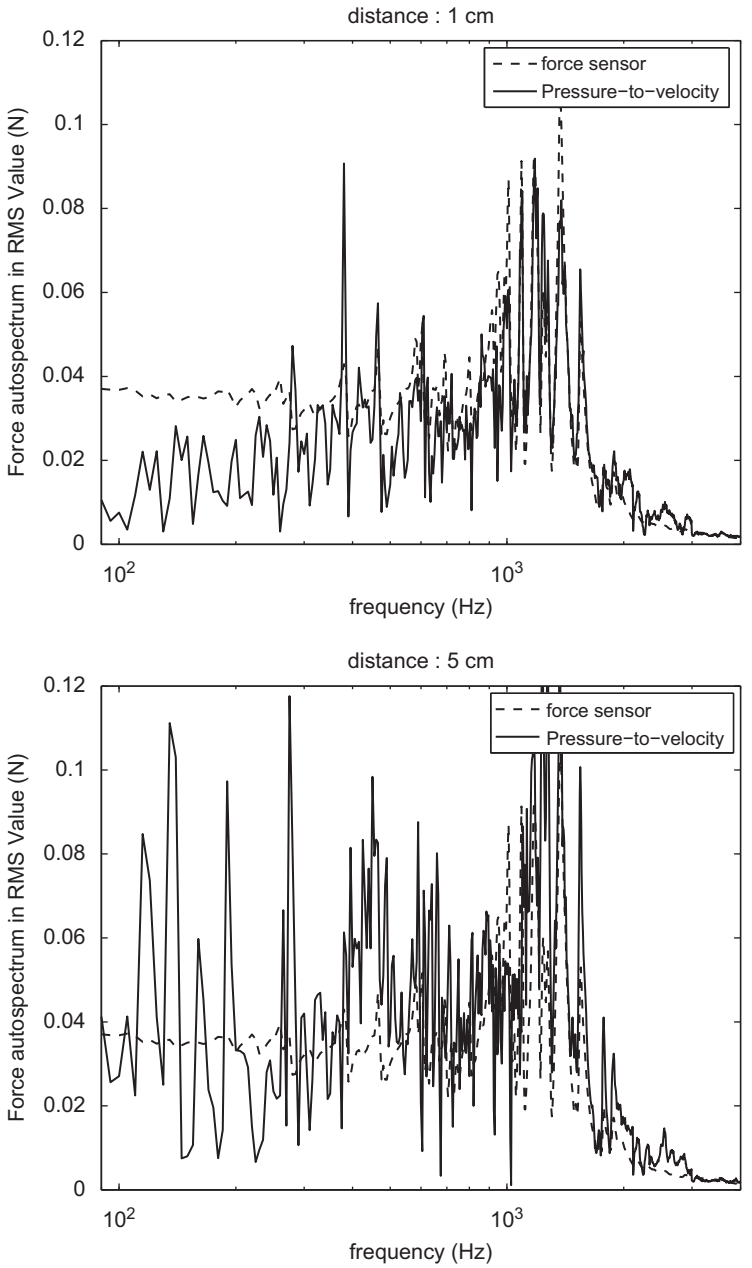

Fig. 21. Force spectra. Dotted line: measured by the piezoelectric sensor—solid line: identified by FAT from pressure-to-velocity holography. Up: measurements at 1 cm—down: measurements at 5 cm.

are the same as in the previous section. To calculate the force value (in Newton), the peak observed on force distributions (in N/m^2) is spatially integrated by the discretized equation:

$$F = \Delta_x \cdot \Delta_y \sum_{i=nf-nl}^{nf+nl-1} \sum_{j=mf-nl}^{mf+nl-1} F_{i,j} \tag{9}$$

where F denotes the complex force value, $F_{i,j}$ is the force distribution at the point indices (i,j), nf and mf the excitation point indices (identified by the maximum of the pic) and nl is the half-length of the spatial response of the FAT filter. Note that this calculation is performed at each frequency, but an automatic procedure is carried out since the excitation point coordinates are determined and the regularization parameters are fixed.

Figs. 20–22 show the force obtained by FAT compared to the force measured by the force sensor (which is the same in all figures). The FAT obtained from laser measurements (Fig. 20) is a reference of what is obtained today with modern

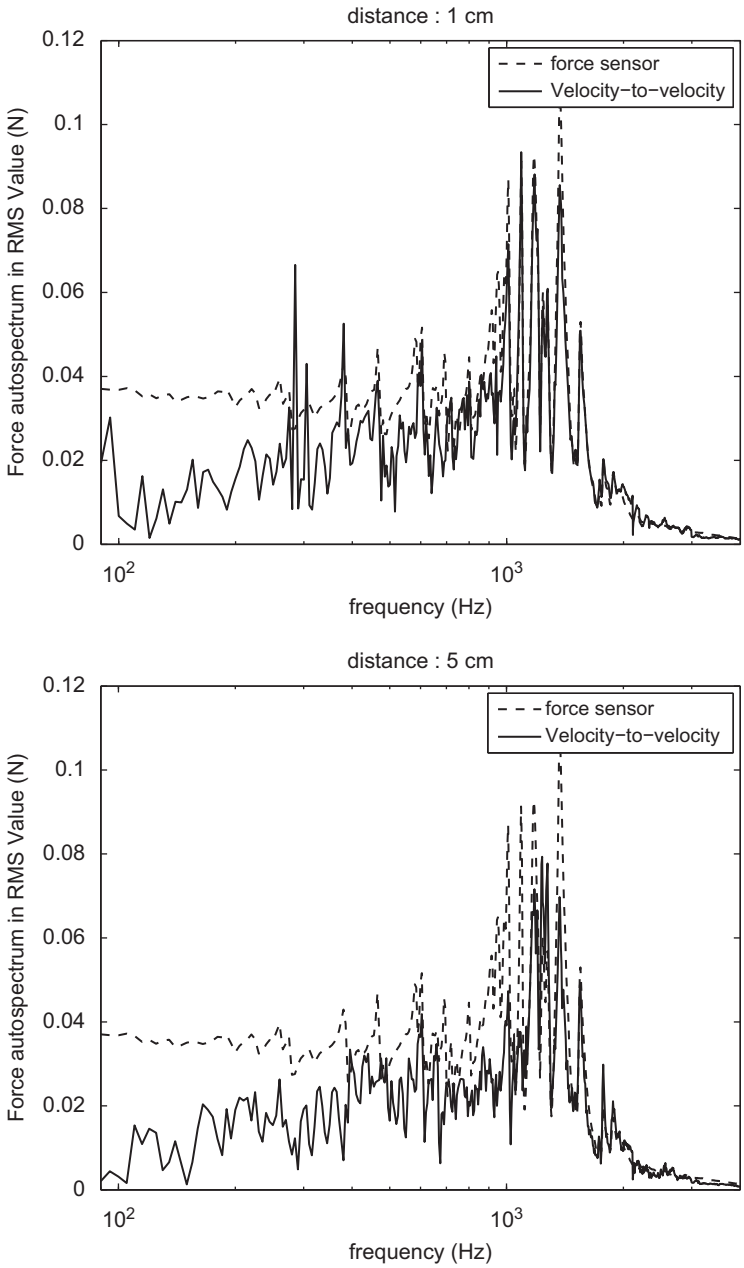

Fig. 22. Force spectra. Dotted line: measured by the piezoelectric sensor—solid line: identified by FAT from velocity-to-velocity holography. Up: measurements at 1 cm—down: measurements at 5 cm.

equipment. The result is excellent, except in the low frequency domain ($f < 300$ Hz), because the area becomes too small in comparison with the wavelength. Indeed, when the window is shorter than one wavelength, the entire force distribution is weighed and the result is underestimated. To overcome this limitation, a larger measurement area is needed.

Concerning FAT on pressure-to-velocity NAH predictions, Fig. 21 allows concluding on the possibility of reconstructing the excitation provided the distance between the structure and measurements is very small. Generally, this approach gives poor quality, but it has the advantage of using microphones which are cheaper than a scanning laser vibrometer or acoustic velocity sensors.

Lastly, Fig. 22 shows that FAT applied on back-propagated acoustic velocity measured by a Microflown p-U probe gives good quality. For a distance of 1 cm (at the top) the differences between curves are comparable to those obtained with the laser vibrometer (Fig. 20). At 5 cm, quality is lower and the force magnitude is underestimated in a wider frequency band ($f < 1500$ Hz). However, the quality is generally good, so that measurements at this distance are conceivable.

5. Conclusion

FAT is a technique that allows locating and identifying vibration excitations in the displacement field of a structure. The method requires numerous vibration responses on a given meshgrid. Contactless measurements are investigated in this paper in order to overcome the difficulty of measurement. The aim was to study the possibility of using acoustic holography so that structure displacement fields can be identified with a movable antenna. The structure studied is a suspended plate excited by a shaker and the test consists in identifying the position and the value of the force. Three kinds of measurements were performed: plate velocities by classic laser measurements, sound pressures at 1 and 5 cm from the plate and acoustic particle velocities at 1 and 5 cm from the plate using the recent sensors developed by Microflown Technologies. Localizations and force identifications lead to the same observations. Firstly, pressure-to-velocity holography can be used, but the distance to the plate must be small. Here, holography can be considered as being similar to a conversion of pressures into velocities. Secondly, velocity-to-velocity holography gives very good results, comparable to those obtained by a laser vibrometer. Here, holography can be seen as back-propagation, making it possible to consider longer distances from the structure. Therefore the use of p-U probe technology is particularly interesting due to its ease of use.

The test considered is of course restricted to point force identification and its generalization to all kinds of excitation is certainly the first direction that should be explored. Other deterministic excitations (such as moments, distributions, etc.) should not be a problem, since FAT is capable of reconstructing a spatially correlated force distribution as a quantity. However, when excitations are uncorrelated (such as turbulent boundary layer excitation), the method cannot be used as it is, but the advantage of contactless measurement with an antenna is that it can acquire fields simultaneously and the same technique developed here can be applied in the temporal domain.

The outlook for further research is promising for other similar techniques. For example, acoustic back-propagations can also be performed by the inverse BEM (boundary element method) method [19], facilitating measurements on geometries different to a plane. Also, the improvement of FAT for use on complex structures by using FEM modeling is an interesting challenge, leading to the extension of the approach to all radiating structures.

References

[1] E.G. Williams, J.D. Maynard, E. Skudrzyk, Sound source reconstructions using a microphone array, *Journal of the Acoustical Society of America* 68 (4) (1980) 340–344.
[2] J.D. Maynard, E.G. Williams, Y. Lee, Nearfield acoustic holography: I. Theory of generalized holography and the development of NAH, *Journal of the Acoustical Society of America* 78 (4) (1985) 1395–1413.
[3] A.W. Veronesi, J.D. Maynard, Nearfield acoustic holography: II. Holographic reconstruction algorithms and computer implementation, *Journal of the Acoustical Society of America* 81 (5) (1987) 1307–1322.
[4] C. Pezerat, Méthode d'identification des efforts appliqués sur une structure vibrante, par résolution et régularisation du problème inverse (Identification of Forces Applied on Vibrating Structures by Resolution and Regularization of the Inverse Problem), Ph.D. Thesis, Institut National des Sciences Appliquées de Lyon, December 1996.
[5] C. Pezerat, J.-L. Guyader, Force analysis technique: reconstruction of force distribution on plates, *Acustica united with Acta Acustica* 86 (2000) 322–332.
[6] C. Pezerat, J.-L. Guyader, Two inverse methods for localization of external sources exciting a beam, *Acta Acustica* 3 (1995) 1–10.
[7] C. Pezerat, J.-L. Guyader, Localisation d'efforts appliqués sur des structures minces; régularisation du problème inverse (localization of forces applied on thin structures; regularization of the inverse problem), Revue Française de Mécanique, 1996, pp. 49–55.
[8] C. Pezerat, T. Loyau, J.-L. Guyader, Power source characterisation using the riff test bench, in *Euronoise 2001*, Patra, Greece, 2001.
[9] M.S. Djamaa, N. Ouelaa, C. Pezerat, J.-L. Guyader, Radial force identification of a finite cylindrical shell by an inverse method, *Acustica united with Acta Acustica* 92 (3) (2006) 398–405.
[10] M.S. Djamaa, N. Ouelaa, C. Pezerat, J.-L. Guyader, Reconstruction of a distributed force applied on a thin cylindrical shell by an inverse method and spatial filtering, *Journal of Sound and Vibration* 301 (3–5) (2007) 560–575.
[11] H.E. De Bree, P. Leussink, T. Korthorst, H. Jansen, T. Lammerink, M. Elwenspoek, The microflown; a novel device measuring acoustical flows, *Sensors and Actuators A—Physical* SNA054 (1–3) (1996) 552–557.
[12] R. Raangs, W.F. Druyvesteyn, H.E. De Bree, A low-cost intensity probe, *Journal of the Audio Engineering Society* 51 (2003) 344–357.
[13] H.E. De Bree, The microflown: an acoustic particle velocity sensor, *Acoustics Australia* 31 (2003) 91–94.
[14] F. Jacobsen, Y. Liu, Near field acoustic holography with particle velocity transducers, *Journal of the Acoustical Society of America* 118 (5) (2005).
[15] F. Jacobsen, Y. Liu, Near field acoustic holography based on an array of particle velocity sensors, in *Internoise 2005*, Rio de Janeiro, Brazil, 7–10 August 2005.

[16] J.S. Bendat, A.G. Piersol, *Engineering Applications of Correlation and Spectral Analysis*, Wiley-Interscience Publication, 1980.
[17] E.G. Williams, *Fourier Acoustics*, Academic Press, New York, 1999.
[18] E.G. Williams, Continuation of acoustic near-fields, *Journal of the Acoustical Society of America* 113 (2003) 1273–1281.
[19] M.R. Bai, Application of bem based acoustic holography to radiation analysis of sound sources with arbitrarily shaped geometries, *Journal of the Acoustical Society of America* 92 (1992) 533–549.